Multidimensional Potential Energy Surfaces resolved at the RASPT2 level for accurate photoinduced isomerization dynamics of azobenzene

Flavia Aleotti,[†,‡] Lorenzo Soprani,[†,‡] Artur Nenov,[*,†] Roberto Berardi,[†] Alberto Arcioni,[†] Claudio Zannoni,[†] and Marco Garavelli[*,†]

[†]*Dipartimento di Chimica Industriale "Toso Montanari", Universitá di Bologna, Viale del Risorgimento 4, 40136 Bologna, Italy*

[‡]*This authors contributed equally to this work*

E-mail: artur.nenov@unibo.it; marco.garavelli@unibo.it

Supporting Information Available

1 Active space orbitals

1.1 *trans*-azobenzene

Occupied orbitals:

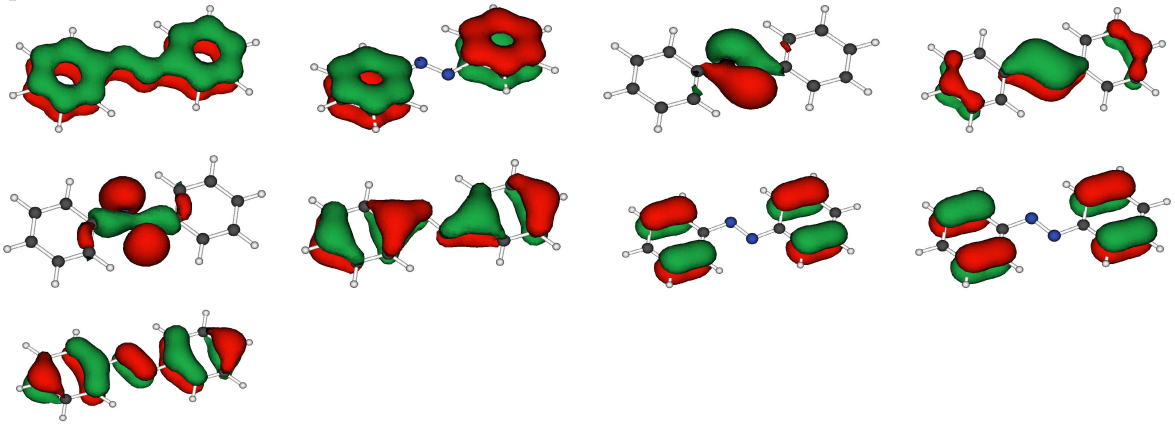

Virtual orbitals:

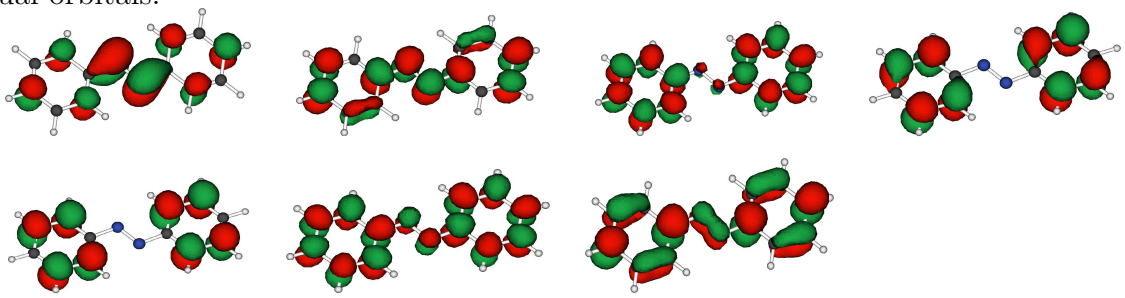

1.2 *cis*-azobenzene

Occupied orbitals:

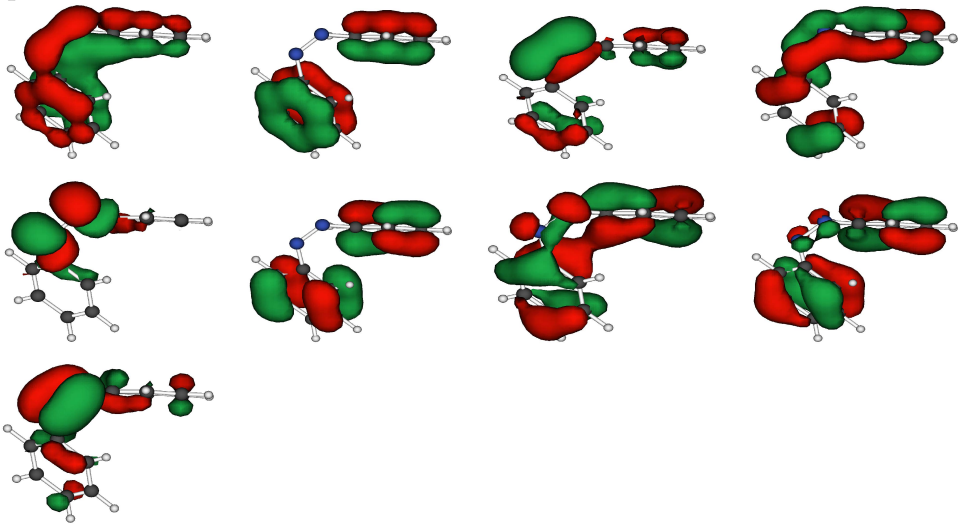

Virtual orbitals:

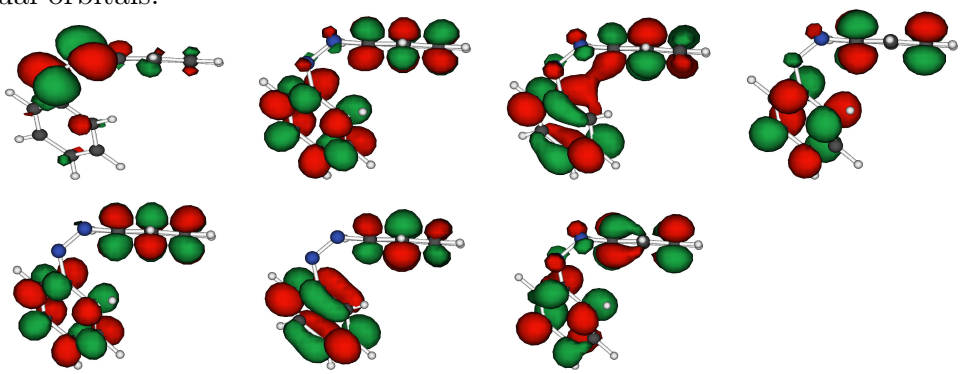

Orbitals involved in the $n\pi^*$ transition:

trans-azobenzene

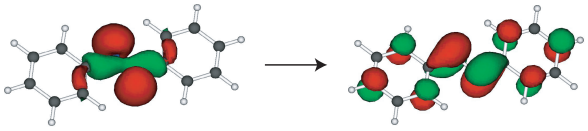

cis-azobenzene

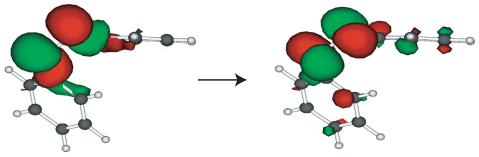

Orbitals involved in the $\pi\pi^*$ transition:

trans-azobenzene

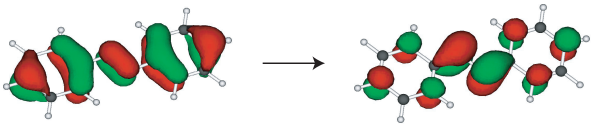

cis-azobenzene

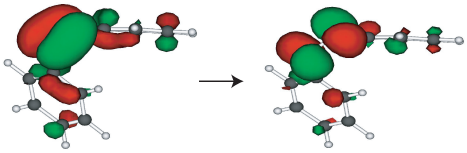

2 SS-RASPT2 *vs* MS-RASPT2

For the points of the rigid scan in which CNNC $< 82°$ or CNNC $> 102°$ the S_0 and S_1 PESs are well separated in energy, and the results of SS-RASPT2 and MS-RASPT2 are exactly the same, as shown in Figure S1 (a). However, for $82° \leq$ CNNC $\leq 102°$, the results of the two methods differ significantly. Here, the SS-RASPT2 PESs show double or triple crossings (see Figure S1 (b)), which disappear after MS-RASPT2 correction. These SS-RASPT2 CIs are not accompanied by a sudden change in the wavefunction, as expected in a real crossing point, but rather the two wavefunctions show a multiconfigurational nature in which the closed shell and $n\pi^*$ configurations mix. This is consequence of the strong wavefunction mixing at the RASSCF level in this region, that is not properly fixed by the SS-RASPT2 correction. However, the scenario is more balanced at MS-RASPT2 level, where the wavefunction mixing is also corrected and the nature of two states is better defined.

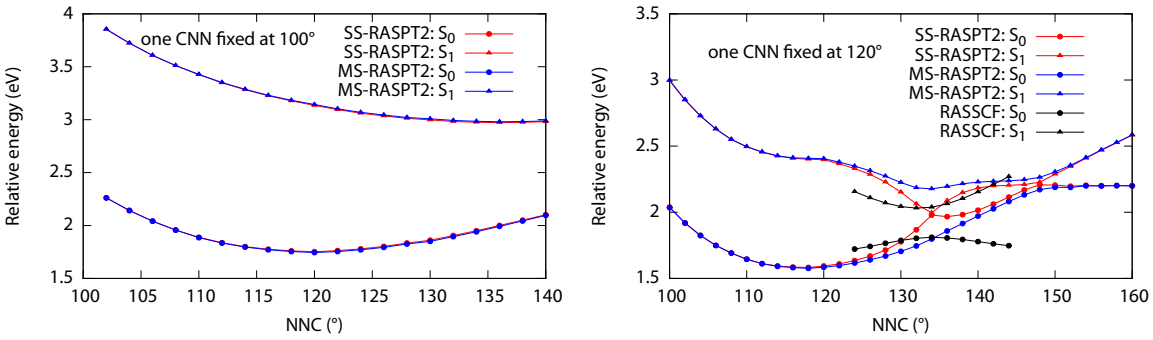

(a) CNNC = 60° (b) CNNC = 90°

Figure S1: Comparison between SS-RASPT2 (red line) and MS-RASPT2 (blue line) energy at CNNC = 60° (a) and at CNNC = 90° (b).

3 Rigid bidimensional scan starting from the *trans* S_0 minimum (torsion + symmetric bending)

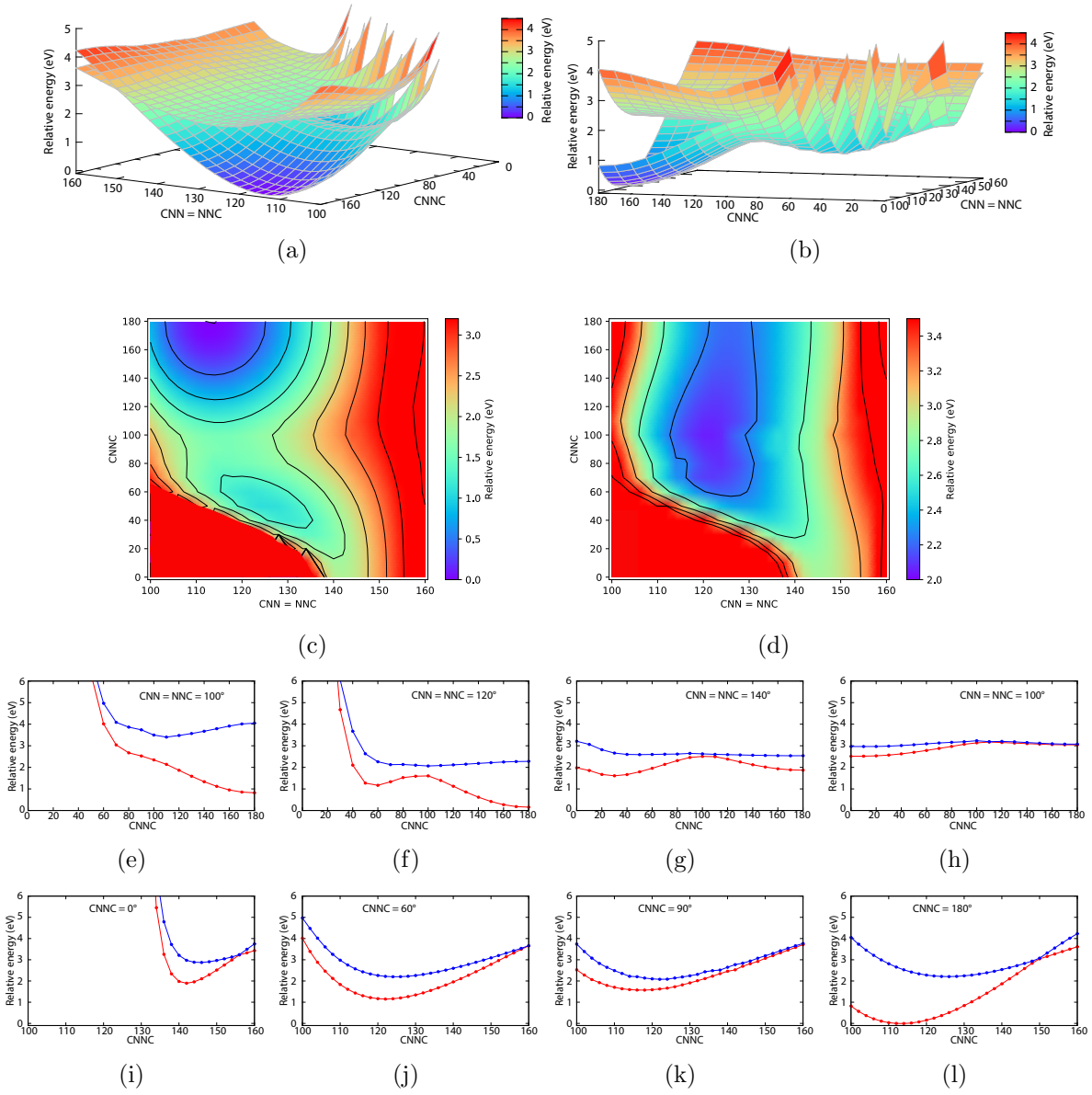

Figure S2: Side views ((a) and (b)) and top view (S_0 (c) and S_1 (d)) of the PESs in the coordinates of CNNC torsion and symmetric CNN bending for the rigid scan starting from the *trans* S_0 minimum; cuts through the PESs for a selected symmetric bending (e-h) and torsion (i-l) values (S_0 red line, S_1 blue line).

4 Rigid bidimensional scan starting from the *cis* S_0 minimum (torsion + symmetric bending)

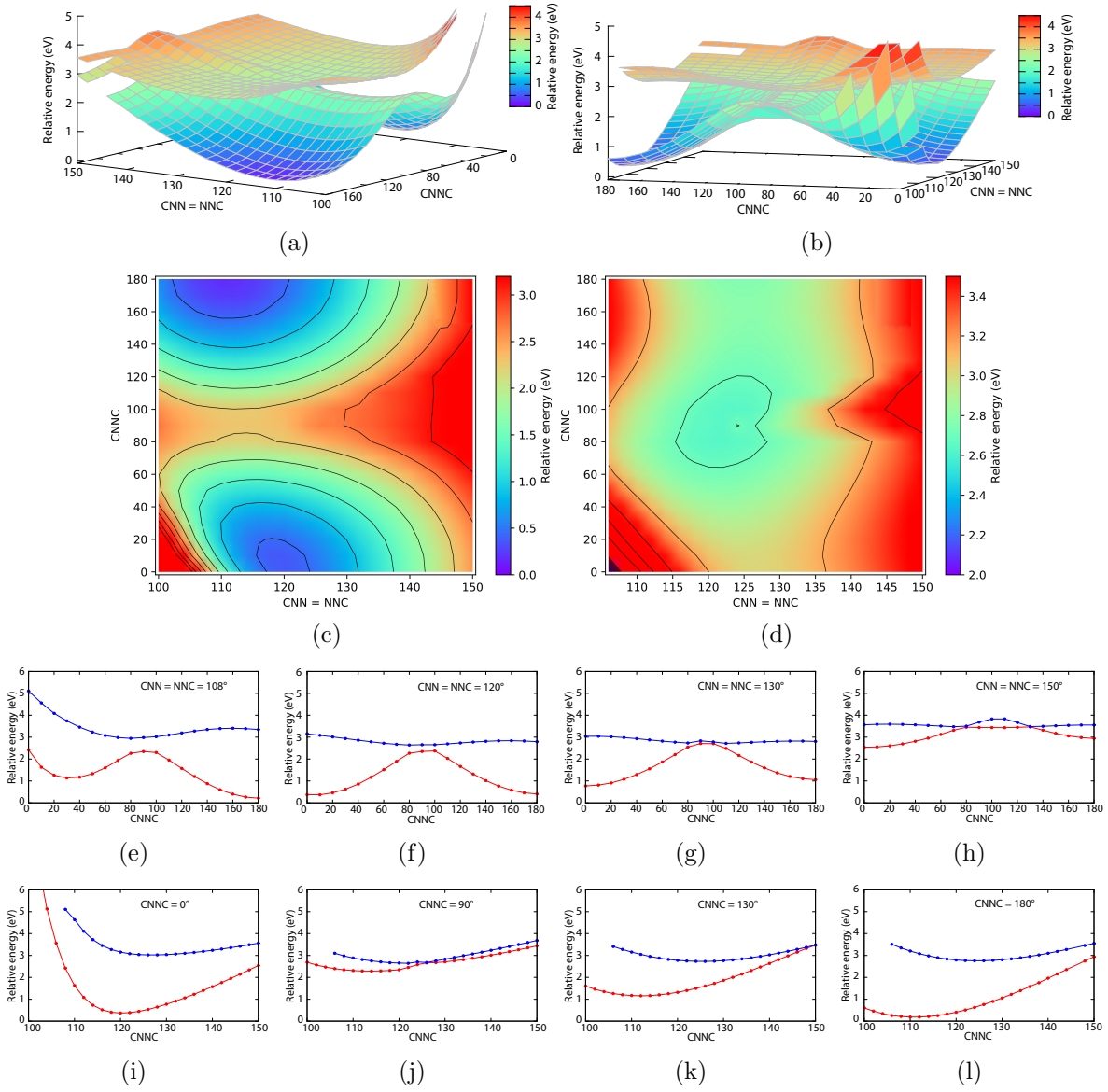

Figure S3: Side ((a) and (b)) and top views (S_0 (c) and S_1 (d)) of the PESs in the space of CNNC torsion and symmetric CNN bending for the rigid scan starting from the *cis* S_0 minimum; cuts through the PESs for a selected symmetric bending (e-h) and torsion (i-l) values (S_0 red line, S_1 blue line).

5 Bidimensional CNN/NNC bending scans

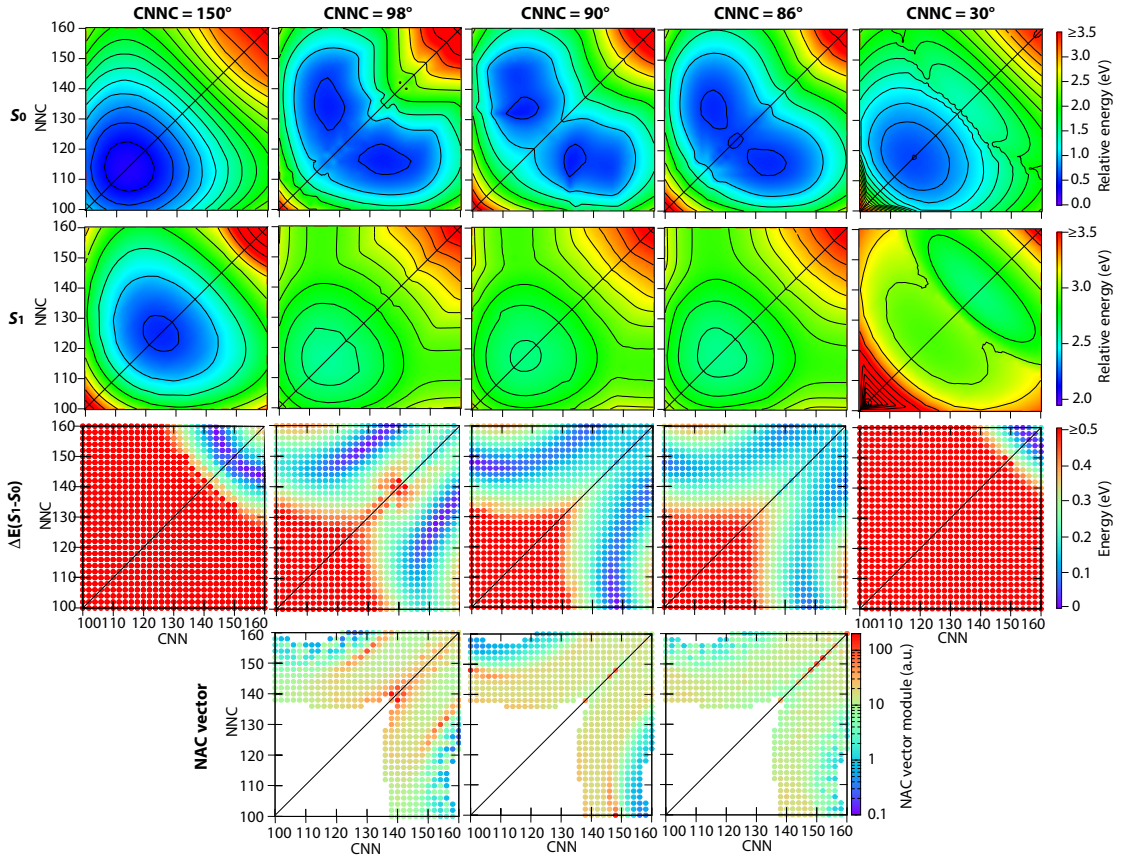

Figure S4: Top views of S_0 and S_1 PESs (isolines every 0.1 eV) and energy gap $E_{S_1-S_0}$ in the space of CNN and NCC bending angles for fixed torsion 150°, 98°, 90°, 86° and 30° at the RASPT2 level (see computational methods); the diagonal connects symmetric structures. For 98°, 90° and 86° torsion the NAC vector module (in atomic units) is also displayed, for the points where $E_{S_1-S_0} \leqslant 0.3$ eV.

For CNNC $\leqslant 60°$ the PESs are affected by the change from *trans*- to *cis*-derived structures, which produces some ridges. This is much visible in the case of CNNC = 10°, where S_1 displays two minima (T10-S_1 min *trans* and T10-S_1 min *cis* see main text): the *trans*-derived structure is the absolute minimum but this is likely to be an artifact of merging the two rigid scans, while the real minimum is more probably the *cis*-derived one, which is more coherent with the $n\pi^*$ minima from the other scans.

5.1 Relevant structures from the rigid scan

Table S1: Structures and energies* of S_0, S_1 and S_2 at significant points (minima, saddle points, relevant CIs) obtained with the rigid scan (in the space of CNNC torsion and CNN/NNC bending) and with unconstrained optimizations. (* a=SS-RASPT2, b=MS-RASPT2)

		CNNC (°)	CNN (°)	NNC (°)	E_{S_0} (eV)	E_{S_1} (eV)	E_{S_2} (eV)
rigid scan of CNNC, CNN = NNC	S_0 *trans* min	180	112-114	112-114	0.00^a	2.66^a	3.86^a
	S_0 *cis* min	0	120	120	0.37^a	3.15^a	-
	S_0 TS	90	118	118	1.57^a	2.14^a	-
	S_1 *trans* min	180	126	126	0.51^a	2.21^a	-
	S_1 *cis* min	0	126	126	0.53^a	3.03^a	-
	S_1 symm min	100	120	120	1.60^a	2.06^a	-
	S_2 min	180	108-110	108-110	0.11^a	2.99^a	3.84^a
	S_1/S_0 CI-bend1	180	150	150	3.04^a	3.08^a	-
	S_1/S_0 CI-bend2	0	156	156	3.22^a	3.24^a	-
rigid scan of CNN, NNC	T120-S_0 min	120	114	114	1.03^a	2.27^a	-
	T120-S_1 min	120	122	122	1.19^a	2.10^a	-
	T102-S_0 min	102	116	116	1.51^b	2.13^b	-
	T102-S_1 min	102	120	122	1.55^b	2.15^b	-
	T94-S_0 min	94	116	116	1.54^b	2.42^b	-
	T94-S_1 min	94	116	132	1.74^b	2.16^b	-
	T82-S_0 min	82	116	116	1.45^b	2.42^b	-
	T82-S_1 min	82	116	134	1.70^b	2.17^b	-
	T60-S_0 min	60	122	122	1.15^a	2.22^a	-
	T60-S_1 min	60	124	124	1.16^a	2.20^a	-
	T10-S_0 min	10	118	118	0.37^a	3.16^a	-
	T10-S_1 min *trans*	10	144	146	2.01^a	2.85^a	-
	T10-S_1 min *cis*	10	126	126	0.57^a	3.01^a	-
	T98-S_1/S_0 CI	98	116	146	2.12^b	2.22^b	-
	T94-S_1/S_0 CI	94	114	146	2.16^b	2.19^b	-
	T90-S_1/S_0 CI	90	114	146	2.13^b	2.20^b	-
	opt-S_1 min	96	115	145	1.98^b	1.98^b	-
	opt-S_1/S_0 CI	95	115	146	1.98^b	1.99^b	-

6 MS-2-RASPT2/SA-2-RASSCF(4,9|0,0|4,7)/ANO-L-VDZP optimized geometries

opt-S_1 min

C	-0.006985	-0.232103	0.090283
C	0.030078	-0.003127	1.486433
C	1.252379	0.190744	2.162892
C	2.455494	0.155297	1.436536
C	2.430874	-0.074810	0.045434
C	1.199922	-0.272303	-0.622270
N	-1.137080	-0.012100	2.305518
N	-2.234636	-0.056160	1.680159
C	-3.214394	-0.852850	1.216864
C	-4.430584	-0.300318	0.717809
C	-5.409036	-1.155837	0.194474
C	-5.216724	-2.555787	0.157453
C	-4.010619	-3.095529	0.655197
C	-3.004798	-2.269254	1.175991
H	-4.581059	0.781159	0.756596
H	-6.339916	-0.723865	-0.185276
H	-5.991023	-3.210603	-0.247706
H	-3.847685	-4.177693	0.637795
H	-2.066231	-2.680039	1.555233
H	1.234137	0.364557	3.242026
H	3.408451	0.308962	1.949978
H	3.366423	-0.100028	-0.519650
H	1.188202	-0.452524	-1.700896
H	-0.968334	-0.375943	-0.406832

opt-S_1/S_0 CI

C	-0.017837	-0.210072	0.092072
C	0.027308	0.004079	1.490481
C	1.254511	0.182461	2.162339
C	2.454150	0.143350	1.430040
C	2.421296	-0.075909	0.037229
C	1.185289	-0.254775	-0.626381
N	-1.135888	-0.012378	2.317480
N	-2.235221	-0.059299	1.697275
C	-3.212787	-0.854912	1.223866
C	-4.419818	-0.302452	0.705234
C	-5.394479	-1.158673	0.175683
C	-5.206229	-2.559044	0.150614
C	-4.009656	-3.097953	0.671105
C	-3.008775	-2.270912	1.201019
H	-4.567254	0.779766	0.733018
H	-6.318479	-0.726204	-0.219801
H	-5.975899	-3.214502	-0.262491
H	-3.848851	-4.180497	0.663513
H	-2.077584	-2.681470	1.598484
H	1.243646	0.343627	3.243481
H	3.410745	0.282156	1.940970
H	3.353962	-0.108282	-0.532208
H	1.166523	-0.425297	-1.706432
H	-0.981816	-0.342961	-0.402548

7 Non-adiabatic couplings

Figure S5: NAC vector coordinates (expressed as x,y,z respectively for each atom) for selected test geometries. The blue color refers to nitrogen atoms while the green color refers to carbon atoms. The x,y,z NAC value for all the hydrogen atoms was always close to 0,0,0 (not reported)

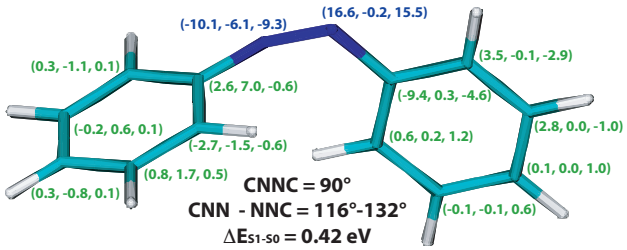

(a)

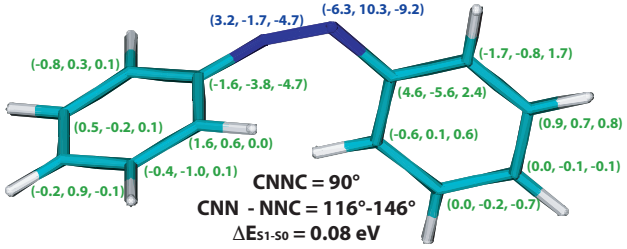

(b)

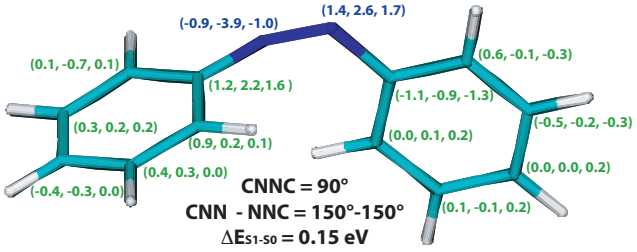

(c)

8 Semiclassical dynamics

8.1 PES fit details

The function ΔU_{tbb} used to reproduce the QM PES is a combination of sixth order cosine and sixth order polynomial approximations

$$\begin{aligned}\Delta U_{\mathrm{tbb}} = U_{\mathrm{tbb}\,0} + U_{\mathrm{t}}(\varphi) + \sum_{i=1}^{2} U_{\mathrm{b},i}(\vartheta_i) + U^{\mathrm{II}}_{\mathrm{bb}}(\vartheta_1,\vartheta_2) + \\ + \sum_{i=1}^{2} U^{\mathrm{II}}_{\mathrm{tb},i}(\varphi,\vartheta_i) + U^{\mathrm{II}}_{\mathrm{btb}}(\varphi,\vartheta_1,\vartheta_2)\,.\end{aligned} \tag{1}$$

The term $U_{\mathrm{tbb}\,0}$ is a shift constant, while

$$U_{\mathrm{t}}(\varphi) = \sum_{n=1}^{6} k_n \cos\left(n\,\varphi - \gamma_n\right) \tag{2}$$

is the expression used to calculate the classical torsional potential energy. The third and the fourth terms,

$$U_{\mathrm{b}i}(\vartheta_i) = \sum_{m=1}^{6} k_i^m \vartheta_i^m\,, \tag{3}$$

$$U^{\mathrm{II}}_{\mathrm{bb}}(\vartheta_1,\vartheta_2) = \sum_{l=1}^{3}\sum_{m=l}^{6-l}\left(k^{l,m}\vartheta_1^l\vartheta_2^m + k^{m,l}\vartheta_1^m\vartheta_2^l\right), \tag{4}$$

are the diagonal and off-diagonal terms of the 2D polynomial approximation and describe the anharmonicity and the coupling (denoted by the superscript II) between the two bending angles ϑ_1 and ϑ_2. The last terms,

$$U^{\mathrm{II}}_{\mathrm{tb}i}(\varphi,\vartheta_i) = \sum_{m=1}^{6}\vartheta_i^m \sum_{n=1}^{6} k_{i,n}^m \cos\left(n\,\varphi - \gamma_n^m\right), \tag{5}$$

$$U^{\mathrm{II}}_{\mathrm{btb}}(\varphi,\vartheta_1,\vartheta_2) = \sum_{l=1}^{3}\sum_{m=l}^{6-l}\sum_{n=1}^{6}\left(k_n^{l,m}\vartheta_1^l\vartheta_2^m + k_n^{m,l}\vartheta_1^m\vartheta_2^l\right)\cos\left(n\,\varphi - \gamma_n^{l,m}\right), \tag{6}$$

are combinations of cosine and polynomial expressions, describing the coupling between the dihedral angle φ and the two bending angles ϑ_1 and ϑ_2. Thus, rewriting equation (1), we get

$$\begin{aligned}\Delta U_{\mathrm{tbb}} = U_{\mathrm{tbb}\,0} &+ \sum_{n=1}^{6} k_n \cos\left(n\,\varphi - \gamma_n\right) + \\ &+ \sum_{i=1}^{2}\sum_{m=1}^{6} k_i^m \vartheta_i^m + \sum_{m=1}^{3}\sum_{n=m}^{6-m} \left(k^{l,m}\vartheta_1^l\vartheta_2^m + k^{m,l}\vartheta_1^m\vartheta_2^l\right) + \\ &+ \sum_{i=1}^{2}\sum_{m=1}^{6} \vartheta_i^m \sum_{n=1}^{6} k_{i,n}^m \cos\left(n\,\varphi - \gamma_n^m\right) + \\ &+ \sum_{l=1}^{3}\sum_{m=l}^{6-l}\sum_{n=1}^{6} \left(k_n^{l,m}\vartheta_1^l\vartheta_2^m + k_n^{m,l}\vartheta_1^m\vartheta_2^l\right)\cos\left(n\,\varphi - \gamma_n^{l,m}\right),\end{aligned} \tag{7}$$

Equation (7) presents 277 parameters, but those to be calculated through the fit procedure can be drastically reduced if applied to our specific problem. Phases γ_n, γ_n^m and $\gamma_n^{l,m}$ can assume the value of 0 or $\pi/2$, but after few tests, we noted that better results were reached keeping all the phases equal to zero. Furthermore, ΔU_{tbb} must be symmetric upon exchange of ϑ_1 and ϑ_2, therefore $k_1^m = k_2^m \equiv k^m$, $k^{l,m} = k^{m,l} \equiv k^{l,m}$, $k_{1,n}^m = k_{2,n}^m \equiv k_n^m$ and $k_n^{l,m} = k_n^{m,l} \equiv k_n^{l,m}$. Thus, we obtain

$$\begin{aligned}\Delta U_{\mathrm{tbb}} = U_{\mathrm{tbb}\,0} &+ \sum_{n=1}^{6} k_n \cos\left(n\,\varphi\right) + \sum_{m=1}^{6} k^m \left(\vartheta_1^m + \vartheta_2^m\right) + \\ &+ \sum_{l=1}^{3}\sum_{m=l}^{6-l} k^{l,m}\left(\vartheta_1^l\vartheta_2^m + \vartheta_1^m\vartheta_2^l\right) + \\ &+ \sum_{m=1}^{6}\left(\vartheta_1^m + \vartheta_2^m\right)\sum_{n=1}^{6} k_n^m \cos\left(n\,\varphi\right) + \\ &+ \sum_{l=1}^{3}\sum_{m=l}^{6-l}\left(\vartheta_1^l\vartheta_2^m + \vartheta_2^l\vartheta_1^m\right)\sum_{n=1}^{6} k_n^{l,m}\cos\left(n\,\varphi\right),\end{aligned} \tag{8}$$

in which the parameters to fit are 112.

The fit has been carried out with the `scipy.optimize.curve_fit` function of Python

(which uses the non linear least squares method), obtaining satisfactory results. Figure S6 shows the fitted surfaces of S_0 and S_1, as well as the comparison between the fitting function and the computed points for selected cuts of the 3D surfaces.

Table S2: Root Mean Square Absolute Error (RMSAE) and Root Mean Square Relative Error (RMSRE) for the fit of S_0 and S_1 PESs

	RMSAE (eV)	RMSRE (%)
S_0	0.049	2.4
S_1	0.042	1.6

8.2 Velocity scaling factor

Since the molecule has only three non-frozen degrees of freedom, the atoms velocities will be significantly smaller with respect to a fully unconstrained simulation. This implies a smaller decay probability, due to the presence of a dot product between NAC and velocity in its formula. For this reason, we compared our average velocity of the four central C, N, N, C atoms ($\bar{v}_{\mathrm{R}}$) with that of a Wigner sampling in the full coordinate space ($\bar{v}_{\mathrm{F}}$), finding that

$$\frac{\bar{v}_{\mathrm{F}}}{\bar{v}_{\mathrm{R}}} \approx 4.5 \tag{9}$$

This material is available free of charge via the Internet at `http://pubs.acs.org/`.

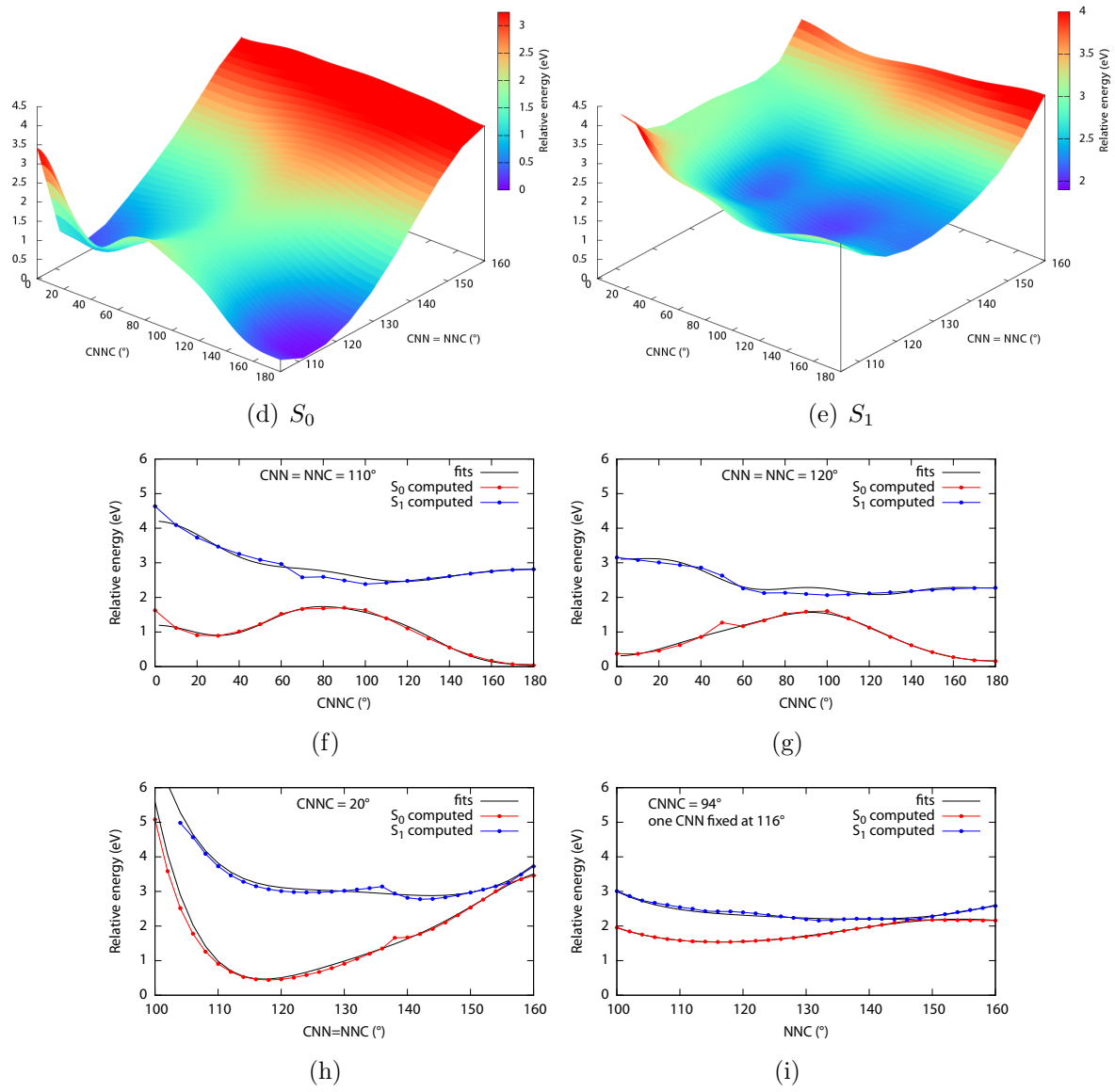

Figure S6: Side views of the fitted S_0 (a) and S_1 (b) PESs in the space of CNNC torsion and symmetric CNN bending; selected cuts through the PESs showing both the computed points and the fit.